How to cite: Angew. Chem. Int. Ed. 2020, 59, 16366–16370
International Edition: doi.org/10.1002/anie.202004447
German Edition: doi.org/10.1002/ange.202004447

Molecular Machines | Hot Paper

Regeneration of Burnt Bridges on a DNA Catenane Walker

Julián Valero and Michael Famulok**

Dedicated to Professor Bernd Giese on the occasion of his 80th birthday

Abstract: *DNA walkers are molecular machines that can move with high precision onthe nanoscale due to their structural and functional programmability. Despite recent advances in the field that allow exploring different energy sources, stimuli, and mechanisms of action for these nanomachines, the continuous operation and reusability of DNA walkers remains challenging because in most cases the steps, once taken by the walker, cannot be taken again. Herein we report the path regeneration of a burnt-bridges DNA catenane walker using RNase A. This walker uses a T7RNA polymerase that produces long RNA transcripts to hybridize to the path and move forward while the RNA remains hybridized to the path and blocks it for an additional walking cycle. We show that RNA degradation triggered by RNase A restores the path and returns the walker to the initial position. RNase inhibition restarts the function of the walker.*

Biological molecular motors are complex proteins, powered by chemical energy, which are capable of generating directional movement and performing specific work.[1,2] In living organisms, directional motion is used for a wide variety of complex and essential functions like cargo transport, cell locomotion and division, and nucleic acid polymerization. Misfolding or mutations in these protein machines can result in severe diseases or lethality.

Early examples of synthetic motors based on switchable small-molecule assemblies paved the way for designing systems with complex functionalities resembling or mimicking these proteins.[3] Since the recent advent of protein engineering and especially DNA nanotechnology, efforts focused on modifying or mimicking natural molecular motors in order to create biohybrid structures that move efficiently with nanometer precision, high directionality, and processivity.[4] DNA walkers,[5] rotors,[6] and synthetic protein:DNA nanohybrids[4f] powered by a wide range of external stimuli have been described, showing potential applications in the transport and release of biological cargoes,[7] cargo sorting,[8] single-molecule detection, organic synthesis,[9] biosensing and circuits,[5a,7a,10] and therapy.[11] On one hand, these artificial systems can shed light on the structural and dynamic physicochemical properties of natural molecular motors and how they work in the cellular environment. On the other hand, novel structural and functional elements from which these molecular machines are constructed allow exploring new forms of motion, alternative and more efficient fuel sources than ATP (i.e. light,[12] ultrasound,[13] electric field[14] or other more efficient and cost-effective chemical inputs[5b,15]), potential applications in synthetic environments, and how the performance of these motors can be improved.

Interlocked molecules bear enormous potential for the design and construction of artificial molecular motors.[16] We have recently reported a biohybrid DNA catenane walker based on a rotatory nanoengine that upon rolling-circle transcription (RCT) harnesses the long RNA transcript produced to perform linear motion.[17] To that end, an engineered T7RNA polymerase fused to a zinc finger protein (zif268) powers the nanoengine. The protein tightly binds to a sequence encoded in one of the DNA rings of the catenane—defined as the stator—which is specifically recognized by the zinc finger domain (Figure 1, Scheme S1 and Table S1 in the Supporting Information). The other catenated ring—the rotor—encodes the T7 promoter sequence and therefore can be transcribed by the T7RNA polymerase in the presence of nucleoside triphosphates (NTPs) fuel. The stator ring contains a protruding single-stranded (ss) DNA strand with two different domains (Figure 1, green and red) that permit the nanoengine to hybridize with two distinct positions, termed Step1 and Step2, within a DNA path. The DNA path consists of a six-helix bundle DNA origami nanotube which contains overhanging ssDNA strands, termed intermediate steps (iSteps), designed to allow the hybridization of the catenane walker and the RNA that is produced during RCT (Table S2 in the Supporting Information). Prior to transcription, the catenane walker preferentially hybridizes to an initial position, defined as Step1, by employing the ssDNA red domain. Upon addition of NTPs, the T7RNA polymerase

[*] Dr. J. Valero, Prof. Dr. M. Famulok
LIMES Chemical Biology Unit, Universität Bonn
Gerhard-Domagk-Straße 1, 53121 Bonn (Germany)
and
Center of Advanced European Studies and Research
Ludwig-Erhard-Allee 2, 53175 Bonn (Germany)
E-mail: julianval10@hotmail.com
m.famulok@uni-bonn.de

Dr. J. Valero
Present address:
Interdisciplinary Nanoscience Center—INANO-MBG, iNANO-huset
Gustav Wieds Vej 14, building 1592, 328, 8000 Aarhus C (Denmark)

Supporting information (including experimental details) and the ORCID identification number(s) for the author(s) of this article can be found under: https://doi.org/10.1002/anie.202004447.

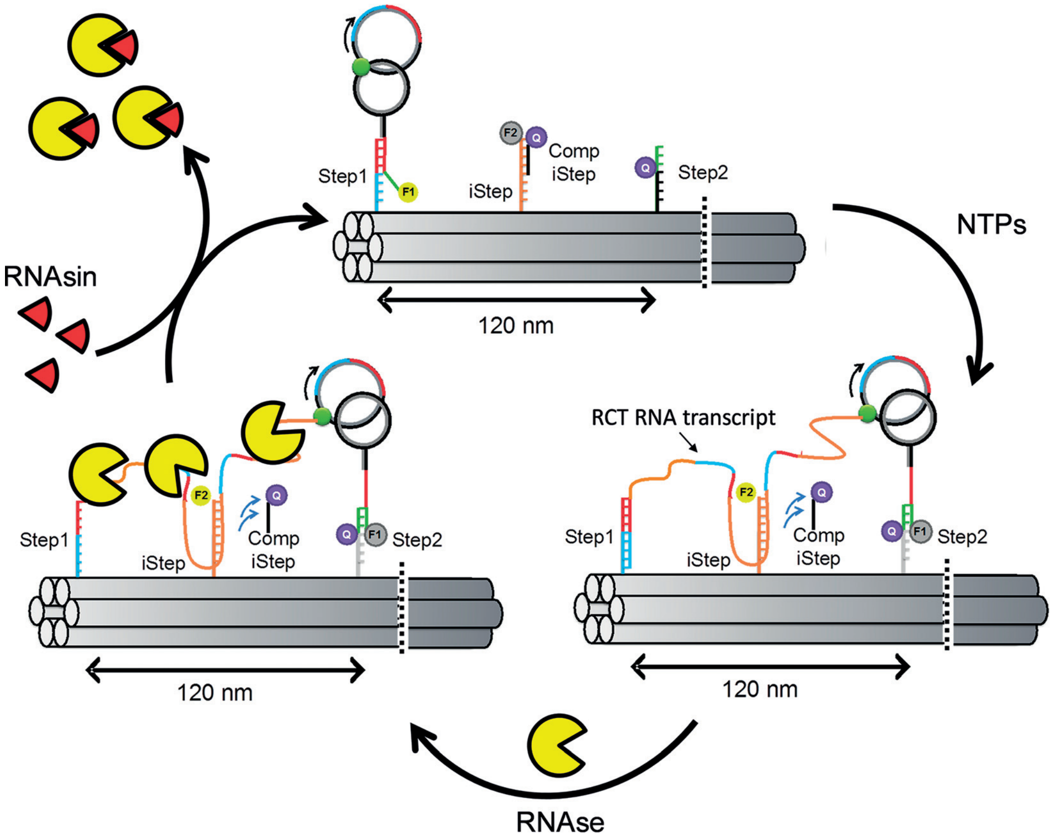

Figure 1. Schematic representation of the walking and enzymatic path regeneration mechanism of a burnt-bridge DNA catenane nanoengine. The 5′ end of the catenane walker overhang was labeled with a TAMRA (F1) fluorophore, whereas Step2 held the complementary black-hole quencher (BHQ-2 [Q]). In parallel, the intermediate step (iStep) was labeled with Cy5 (F2) and its complementary ODN (comp-iStep) with BHQ-3. Note that the comp-iStep quencher ODN does not participate in the walking process, but its strand displacement and release into the bulk is used to monitor the binding of the transcribed RNA to the iStep and thus, the walking progression. At the beginning of a walking cycle, the nanoengine is hybridized to Step1. Upon addition of NTPs RCT can start and the nanoengine walks along the track in a directional way.[17b] Step1, all iSteps and, finally, Step2 cannot serve as steps once the engine has bound to them, because the RNA remains hybridized. Addition of RNase (yellow PacMan) selectively digests the RNA, thus removing the blockade on the steps. Finally, after inhibition of the RNase by addition of RNasin (red triangle), each formerly burnt bridge becomes accessible for a new walking cycle. F1: TAMRA fluorophore; F2: Cy5 fluorophore; Q: Black-hole quenchers (BHQ-2 or BHQ-3).

starts transcription and the generated RNA first binds to the Step1, resulting in the displacement of the catenane from the initial position. Elongation of the RNA transcript during RCT and its hybridization to intermediate steps (iSteps) guide the unidirectional movement of the catenane walker on the DNA path.

Finally, when enough RNA is generated, the catenane walker reaches Step2, hybridizing to it via the ssDNA green domain. This nanostructure is capable of directional, processive, and efficient walking for up to ca. 240 nm. However, since the RNA remains bound to the steps, all steps are blocked after a single walking cycle, preventing their repeated use. Our nanoengine shares this drawback with other DNA walkers in which the path is degraded by selective cleavage or blocked with complementary fuel DNA strands.[18] These "burnt bridges" prevent the walker from moving backwards, reusing the DNA path, performing consecutive walking cycles, or allowing several nanoengines to walk along the same path. Thus, compared with naturally occurring molecular motors, artificial ones suffer from the shortcomings of low turnover numbers and lack of reusability that limit their applicability. Due to the use of RNA to direct the movement of the catenane walker, our system holds potential for restoring a burnt bridge, by employing RNA degradation as a means for liberating the ssDNA-steps to allow continuous operation or multiple walking cycles.

Herein we describe the enzymatic regeneration of an RNA burnt-bridge path to perform consecutive walking operations. We sequentially employed RNase to degrade the RNA that blocks the steps of the DNA path, and RNasin to successively inhibit the RNase, thus allowing the catenane walker to return to its initial position (Step1) and start transcription again. Different fluorophore labels were incorporated into the nanoengine and the path as shown previously[17b] in order to monitor the changes in position of the catenane walker and the hybridization of the RCT transcript on the DNA origami path.

First, we investigated the regeneration of the DNA path by employing different RNases on our catenane walker system. RNases H and A, and a mix of RNases A and T1 were evaluated to test the degradation of the RNA produced during rolling-circle transcription after a full walking cycle. RNase H hydrolyzes RNA in DNA:RNA duplexes, thus degrading the RNA fragments that hybridize with the steps of the path, whereas RNase A specifically hydrolyzes RNA at pyrimidines (U and C) and RNase T1 at G nucleobase.[19]

The walking and path regeneration processes, that is, the return of the DNA catenane walker to Step1, were monitored by fluorescence measurements (Figure 2). After addition of NTPs, the catenane walker initially moves from the starting position (Step1) to the final position (Step2), separated by 120 nm distance, with the generated RNA progressively

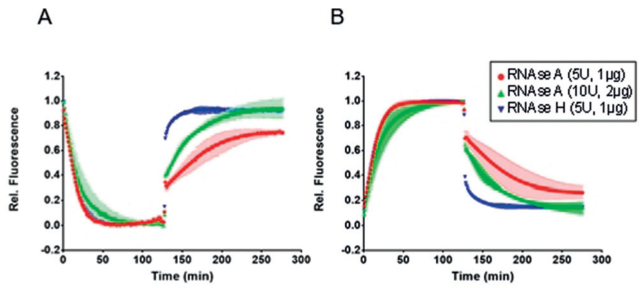

Figure 2. RNases A and H effectively regenerate the burnt-bridge track. A) Normalized TAMRA fluorescence signal (F1) of the catenane walker after a walking cycle and addition of RNases A and H at $t=130$ min. B) Normalized Cy5 fluorescence signal of iSteps. Red and blue curves account for the experiments performed using 1 μg and 2 μg of RNase A, respectively, whereas the green curve corresponds to the addition of 1 μg of RNAse H after a walking cycle. Data are presented as mean ± s.d. $n=2$.

hybridizing to the intermediate step. We observed complete quenching of the catenane walker fluorescence signal (F1, TAMRA) upon reaching Step2 and the increase of the Cy5 fluorescence signal (F2) of iStep, thus indicating that the walker performed a full walking cycle (Figure 2 A). RNase A and RNase H were individually added at $t=130$ min, and full recovery of the initial fluorescence signal readout was effectively observed, confirming the degradation of the RNA. This allows the walker to return to the initial Step1 position as hybridization of the catenane walker overhang to the Step2 position is considerably weaker than to Step1, which contains a toehold involving more base pairs with the walker. Control experiments (Figure S1 in the Supporting Information) show that the catenane walker is stable in Step1 and Step2 positions during the walking and regeneration processes depending on the input conditions.

At equimolar concentrations, RNase H exhibits faster kinetics in RNA degradation and path regeneration than RNase A (Step2→Step1 transition half-lives (τ) of 4.9 and 26.9 min, respectively), whereas no significant differences were observed between RNase A and the A/T1 mixture (Figure S2 in the Supporting Information). However, we finally selected RNase A to regenerate the DNA path due to the lack of effective and commercially available RNase H inhibitors (Figure S3 in the Supporting Information). Note that the path regeneration allows the catenane walker returning non-processively to Step1 of another DNA origami track involved in the strand displacement reaction and therefore, the process is purely governed by Brownian random motion. A less likely, but still feasible, scenario is that the DNA origami track bends, and combined with the flexibility and length of the steps, allow the walker to return to its original Step1 by proximity effects.

Different concentrations of RNase A were systematically tested to optimize the kinetics of path regeneration. As expected, increasing amounts of RNase A yielded faster RNA degradation that is, Step2→Step1 transition kinetics, ranging from half-lives (τ) of 62 ± 18 min to 16 ± 3.4, when using 0.5 μg or 2 μg of RNase A, respectively (Figure 3 A). The amount of RNase A needs to be adjusted allowing the

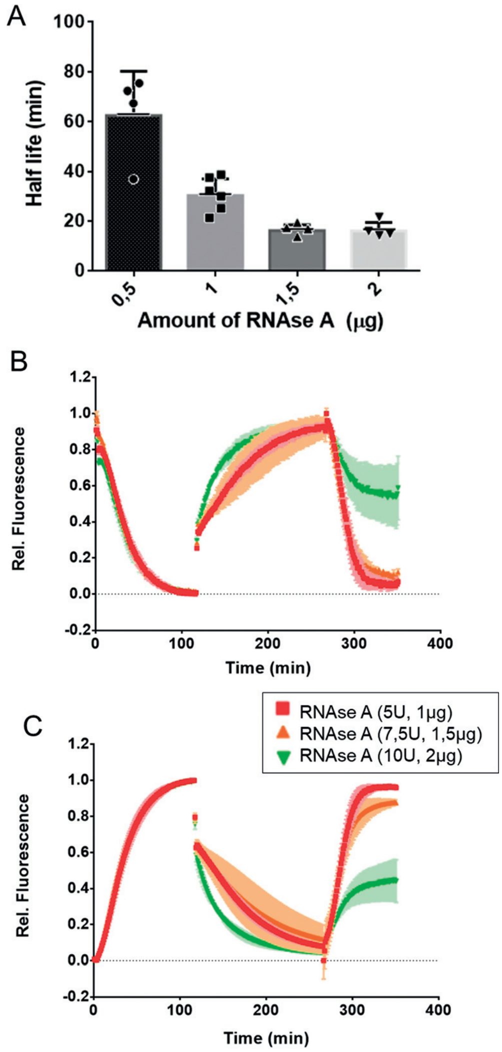

Figure 3. Kinetics of RNA degradation and resetting of catenane walker. A) Half-lives of the Step2→Step1 transition at different concentrations of RNase A. Data are shown as mean ± s.d., $n=4$. B) Normalized fluorescence data of the catenane nanoengine after consecutive steps of walking, regeneration at different RNase A concentrations [$t=117$ min, 1.0 μg (red curves), 1.5 μg (orange curves) and 2 μg (green curves) of RNase A] and walking again ($t=268$ min) monitoring TAMRA fluorescence and C) Cy5 fluorescence. Data are presented as mean ± s.d., $n=2$.

regeneration of the system and subsequent walking cycles. To that end, we employed a commercial recombinant RNase inhibitor (RNasin) that inactivates RNase A by noncovalent binding, thus allowing once again the production of a long rolling-circle RNA transcript that powers the forward motion of the catenane walker. Therefore, the amount of RNase A employed for the path regeneration is restricted to the amount of RNase inhibitor that the system accepts. This limit was empirically determined to be approximately 6 μL (240 U) of RNasin. Higher dilution of the system drastically lowers the efficiency of the walking, affecting both the transcription activity and the hybridization of the catenane walker to the different steps. Therefore, taking into consideration that regeneration of the walker activity is intrinsically linked to the amount of RNase employed, experimentally selected concentrations of RNase A were tested in combination with subsequent addition of RNasin, and supplement of NTPs and T7 RNAP to optimize a second cycle operation of the catenane walker motor (Figure 3B,C).

We found that the optimal amount of RNase A during the second walking cycle was 1.5 µg. When the amount of added RNase A was increased to 2.0 µg (green curve), while the RNasin concentration was held constant, the fluorescence signal reached only about half of the plateau level observed at 1.5 µg RNase A. For instance, the TAMRA (F1) signal is not completely quenched during the second walking cycle, meaning that ca. 60 % of the catenane walker molecules do not efficiently reach Step2. These data clearly suggest that at 2.0 µg RNase A the RNasin concentration is not sufficient to completely inhibit the added amount of RNase A.

Finally, we investigated whether the catenane walker is able to return once again to the starting position of the path after the second walking cycle by successive addition of RNase A. As shown in Figure 4, the TAMRA fluorescence signal of the catenane walker increased again to almost the maximum relative fluorescence. Conversely, the Cy5 fluorescence at the intermediate steps decreased as expected, indicating the degradation of the RNA and hybridization of the complementary quencher oligodeoxynucleotide strands after addition of RNase A. We tested whether further walking cycles would be possible and found that the system considerably fatigued after the second cycle (data not shown), presumably because subsequent addition of RNasin impedes the correct operation of the walker due to increased levels of dilution that counteract transcription and hybridization efficiency.

To conclude, we have shown that it is possible to regenerate a burnt-bridge path in a DNA/RNA walker by enzymatic hydrolysis of the RNA that drives and directs the walker. Our walker design allows that, after completion of a first walking cycle, the efficient hydrolysis of the RNA by RNase A stochastically returns the catenane walker from its end-position back to its starting position. Subsequent addition of RNasin inhibits the RNase A and makes it possible to perform a second walking cycle. Fine-tuning the relative concentration of these proteins is cornerstone for the correct and continuous operation of the DNA walker. The experimental conditions established in this work make it possible to achieve at least two complete alternate cycles of walking and regeneration. Although artificial non-burning bridge molecular motors and walkers are known,[15,20] to our knowledge, the ability to reset a burnt-bridge walker to perform multiple subsequent cycles of walking is unprecedented. The methodology reported herein is straightforward to implement and shows relatively fast regeneration rates compared to the overall kinetic performance of the walker.

Future efforts will be dedicated to overcome current limitations of the system, for example, by employing chemical inhibitors of RNases that are fully compatible with T7RNA polymerase activity.[21] Alternatively, more potent recombinant RNAse inhibitors could be produced and tested in higher concentrations to counteract the reduced efficiency in hybridization that occurs upon dilution of the system, and the length of Step1 could be increased to achieve a more stable DNA/RNA heteroduplex that can form stably under high-dilution conditions. Attachment of the DNA origami track on a solid support combined with the use of a microfluidic device[22] could also allow for the efficient removal of RNase A and thus, regeneration of the system in a different setup. Finally, the combined use of DNAzymes that specifically cleave the RNA regions required for the walking and subsequent blocking (or inactivating) oligonucleotides to restore the function of the walker, will be considered.[18c,d] These strategies will allow multiple path-regeneration cycles and thus a higher number of walking cycles of the DNA-based catenane motor, opening new avenues for more complex functions and enhanced applicability of DNA walkers.

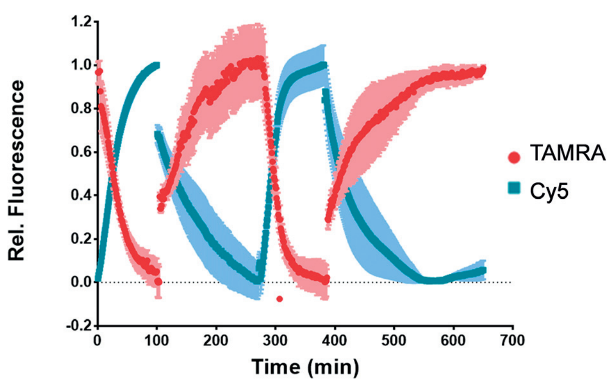

Figure 4. Two consecutive cycles of walking and regeneration. Normalized fluorescence data for Step1→Step2 and Step2→Step1 transitions. Walking and regeneration processes, respectively, are superposed for TAMRA (red curves) and Cy5 fluorophore (blue curves). Data are presented as mean ± s.d., $n = 2$.

Acknowledgements

We thank M. W. Haydell and D. Keppner for experimental help. The research was supported by the Max-Planck-Society and University of Bonn through a Max-Planck-Fellowship to M.F., and the Alexander von Humboldt Foundation (postdoctoral fellowship to J.V.). Open access funding enabled and organized by Projekt DEAL.

Conflict of interest

The authors declare no conflict of interest.

Keywords: biohybrids · DNA catenane walkers · DNA nanotechnology · molecular machines

[1] M. Schliwa, G. Woehlke, *Nature* **2003**, *422*, 759–765.
[2] A. B. Kolomeisky, *J. Phys. Condens. Matter* **2013**, *25*, 463101.
[3] a) S. Kassem, T. van Leeuwen, A. S. Lubbe, M. R. Wilson, B. L. Feringa, D. A. Leigh, *Chem. Soc. Rev.* **2017**, *46*, 2592–2621; b) S. Erbas-Cakmak, D. A. Leigh, C. T. McTernan, A. L. Nussbaumer, *Chem. Rev.* **2015**, *115*, 10081–10206; c) F. Lancia, A. Ryabchun, N. Katsonis, *Nat. Rev. Chem.* **2019**, *3*, 536–551.

[4] a) K. Kinbara, T. Aida, *Chem. Rev.* **2005**, *105*, 1377 – 1400; b) M. Mickler, E. Schleiff, T. Hugel, *ChemPhysChem* **2008**, *9*, 1503 – 1509; c) M. G. van den Heuvel, C. Dekker, *Science* **2007**, *317*, 333 – 336; d) G. Saper, H. Hess, *Chem. Rev.* **2020**, *120*, 288 – 309; e) F. C. Simmel, B. Yurke, H. R. Singh, *Chem. Rev.* **2019**, *119*, 6326 – 6369; f) N. Stephanopoulos, *Chem-Us* **2020**, *6*, 364 – 405.

[5] a) J. Pan, F. R. Li, T. G. Cha, H. R. Chen, J. H. Choi, *Curr. Opin. Biotechnol.* **2015**, *34*, 56 – 64; b) Z. G. Wang, J. Elbaz, I. Willner, *Nano Lett.* **2011**, *11*, 304 – 309; c) F. C. Simmel, *ChemPhysChem* **2009**, *10*, 2593 – 2597.

[6] C. H. Lu, A. Cecconello, I. Willner, *J. Am. Chem. Soc.* **2016**, *138*, 5172 – 5185.

[7] a) T. G. Cha, J. Pan, H. Chen, J. Salgado, X. Li, C. Mao, J. H. Choi, *Nat. Nanotechnol.* **2014**, *9*, 39 – 43; b) H. Gu, J. Chao, S. J. Xiao, N. C. Seeman, *Nature* **2010**, *465*, 202 – 205.

[8] A. J. Thubagere, W. Li, R. F. Johnson, Z. Chen, S. Doroudi, Y. L. Lee, G. Izatt, S. Wittman, N. Srinivas, D. Woods, E. Winfree, L. Qian, *Science* **2017**, *357*, eaan6558.

[9] Y. He, D. R. Liu, *Nat. Nanotechnol.* **2010**, *5*, 778 – 782.

[10] a) Y. K. Xing, B. Liu, J. Chao, L. H. Wang, *RSC Adv.* **2017**, *7*, 47425 – 47434; b) M. A. Boemo, A. E. Lucas, A. J. Turberfield, L. Cardelli, *ACS Synth. Biol.* **2016**, *5*, 878 – 884; c) R. P. Thomsen, M. G. Malle, A. H. Okholm, S. Krishnan, S. S. Bohr, R. S. Sorensen, O. Ries, S. Vogel, F. C. Simmel, N. S. Hatzakis, J. Kjems, *Nat. Commun.* **2019**, *10*, 5655; d) S. S. Wang, A. D. Ellington, *Chem. Rev.* **2019**, *119*, 6370 – 6383; e) D. Wang, C. Vietz, T. Schroder, G. Acuna, B. Lalkens, P. Tinnefeld, *Nano Lett.* **2017**, *17*, 5368 – 5374.

[11] a) F. Li, T. G. Cha, J. Pan, A. Ozcelikkale, B. Han, J. H. Choi, *ChemBioChem* **2016**, *17*, 1138 – 1141; b) R. Jahanban-Esfahlan, K. Seidi, A. Jahanban-Esfahlan, M. Jaymand, E. Alizadeh, H. Majdi, R. Najjar, T. Javaheri, P. Zare, *Nanotechnol. Sci. Appl.* **2019**, *12*, 25 – 46.

[12] a) M. J. Barrell, A. G. Campana, M. von Delius, E. M. Geertsema, D. A. Leigh, *Angew. Chem. Int. Ed.* **2011**, *50*, 285 – 290; *Angew. Chem.* **2011**, *123*, 299 – 304; b) M. X. You, Y. Chen, X. B. Zhang, H. P. Liu, R. W. Wang, K. L. Wang, K. R. Williams, W. H. Tan, *Angew. Chem. Int. Ed.* **2012**, *51*, 2457 – 2460; *Angew. Chem.* **2012**, *124*, 2507 – 2510; c) M. Škugor, J. Valero, K. Murayama, M. Centola, H. Asanuma, M. Famulok, *Angew. Chem. Int. Ed.* **2019**, *58*, 6948 – 6951; *Angew. Chem.* **2019**, *131*, 7022 – 7025.

[13] X. L. Lu, H. Shen, K. D. Zhao, Z. W. Wang, H. M. Peng, W. J. Liu, *Chem. Asian J.* **2019**, *14*, 2406 – 2416.

[14] T. Kudernac, N. Ruangsupapichat, M. Parschau, B. Macia, N. Katsonis, S. R. Harutyunyan, K. H. Ernst, B. L. Feringa, *Nature* **2011**, *479*, 208 – 211.

[15] M. R. Wilson, J. Sola, A. Carlone, S. M. Goldup, N. Lebrasseur, D. A. Leigh, *Nature* **2016**, *534*, 235 – 240.

[16] a) F. M. Raymo, J. F. Stoddart, *NATO ASI Ser. Ser. C* **1996**, *484*, 33 – 51; b) J. F. Stoddart, *Angew. Chem. Int. Ed.* **2014**, *53*, 11102 – 11104; *Angew. Chem.* **2014**, *126*, 11282 – 11284; c) J. Valero, F. Lohman, M. Famulok, *Curr. Opin. Biotechnol.* **2017**, *48*, 159 – 167; d) J. F. Stoddart, *Angew. Chem. Int. Ed.* **2017**, *56*, 11094 – 11125; *Angew. Chem.* **2017**, *129*, 11244 – 11277.

[17] a) F. Lohmann, J. Valero, M. Famulok, *Chem. Commun.* **2014**, *50*, 6091 – 6093; b) J. Valero, N. Pal, S. Dhakal, N. G. Walter, M. Famulok, *Nat. Nanotechnol.* **2018**, *13*, 496 – 503; c) J. Valero, M. Centola, M. Yinzhou, M. Škugor, Z. Yu, M. W. Haydell, D. Keppner, M. Famulok, *Nat. Protoc.* **2019**, *14*, 2818 – 2855.

[18] a) P. Yin, H. Yan, X. G. Daniell, A. J. Turberfield, J. H. Reif, *Angew. Chem. Int. Ed.* **2004**, *43*, 4906 – 4911; *Angew. Chem.* **2004**, *116*, 5014 – 5019; b) J. Bath, S. J. Green, A. J. Turberfield, *Angew. Chem. Int. Ed.* **2005**, *44*, 4358 – 4361; *Angew. Chem.* **2005**, *117*, 4432 – 4435; c) Y. Tian, Y. He, Y. Chen, P. Yin, C. D. Mao, *Angew. Chem. Int. Ed.* **2005**, *44*, 4355 – 4358; *Angew. Chem.* **2005**, *117*, 4429 – 4432; d) K. Lund, A. J. Manzo, N. Dabby, N. Michelotti, A. Johnson-Buck, J. Nangreave, S. Taylor, R. J. Pei, M. N. Stojanovic, N. G. Walter, E. Winfree, H. Yan, *Nature* **2010**, *465*, 206 – 210.

[19] E. A. Barnard, *Annu. Rev. Biochem.* **1969**, *38*, 677 – 732.

[20] a) Z. Wang, R. Hou, I. Y. Loh, *Nanoscale* **2019**, *11*, 9240 – 9263; b) J. Cheng, S. Sreelatha, R. Z. Hou, A. Efremov, R. C. Liu, J. R. C. van der Maarel, Z. S. Wang, *Phys. Rev. Lett.* **2012**, *109*, 238104; c) M. H. Liu, J. Cheng, S. R. Tee, S. Sreelatha, I. Y. Loh, Z. S. Wang, *ACS Nano* **2016**, *10*, 5882 – 5890; d) Y. H. Chiang, S. L. Tsai, S. R. Tee, O. L. Nair, I. Y. Loh, M. H. Liu, Z. S. Wang, *Nanoscale* **2018**, *10*, 9199 – 9211; e) N. Koumura, R. W. Zijlstra, R. A. van Delden, N. Harada, B. L. Feringa, *Nature* **1999**, *401*, 152 – 155.

[21] a) B. D. Smith, M. B. Soellner, R. T. Raines, *J. Biol. Chem.* **2003**, *278*, 20934 – 20938; b) C. C. Earl, M. T. Smith, R. A. Lease, B. C. Bundy, *Bioengineered* **2018**, *9*, 90 – 97.

[22] T. E. Tomov, R. Tsukanov, Y. Glick, Y. Berger, M. Liber, D. Avrahami, D. Gerber, E. Nir, *ACS Nano* **2017**, *11*, 4002 – 4008.

Manuscript received: March 26, 2020
Accepted manuscript online: June 17, 2020
Version of record online: July 20, 2020

